Vol. 6, No. 2, April 2022, pp. 191–195

Current Optics and Photonics

Regular Paper

Lateral Far-field Characteristics of Narrow-width 850 nm High Power GaAs/AlGaAs Laser Diodes

Jung-Tack Yang[1], Jung-Geun Kwak[2], An-Sik Choi[2], Tae-Kyung Kim[2], and Woo-Young Choi[1]*

[1]Department of Electrical and Electronic Engineering, Yonsei University, Seoul 03722, Korea
[2]QSI Inc., Cheonan 31044, Korea

(Received September 23, 2021 : revised December 21, 2021 : accepted December 28, 2021)

We investigate the lateral far-field pattern characteristics, including divergence angle change and far-field pattern analysis as output power increases, of narrow-emitter-width 850 nm GaAs/AlGaAs laser diodes (LDs). Each LD has a cavity of 1200 and 1500 μm and narrow emitter width of 2.4 μm for the top and 4.6 μm for the bottom. The threshold currents are 35 and 40 mA, and L-I kinks appear at power levels of 326 and 403 mW, respectively. The divergence angle tends to increase due to the occurrence of first-order lateral mode and the thermal lensing effect. But with the L-I kink, the divergence angle decreases and the far-field pattern becomes asymmetric. This is due to coherent superposition between the fundamental and the first-order lateral mode. We provide detailed explanations for these observations based on high-power laser diode simulation results.

Keywords : Internal temperature, Kink, Lateral far-field
OCIS codes : (140.2020) Diode lasers; (140.3300) Laser beam shaping

I. INTRODUCTION

The demand for high-power laser diodes (HPLDs) is continuously increasing. Due to their small size, cost-effectiveness, and excellent power conversion efficiency, HPLDs are a key device for emerging new technologies such as LIDAR [1–3] and facial recognition systems [4, 5] and are also widely used as the pumping source for very-high-power laser systems [6–9] for precision machining, medical instruments, and laser weaponry [10–13]. Among the several performance parameters of HPLDs, the output beam quality is essential because it strongly influences free-space beam propagation characteristics, and in the case of using a HPLD as a pumping source, the pumping efficiency.

In many applications, single lateral-mode operation of the HPLD is highly desirable. There are several published reports in which HPLDs with single lateral-mode operation are achieved [14, 15]. For single lateral-mode operation, the laser diodes (LD) must have a narrow emitter width and low lateral confinement. However, in these narrow-width HPLDs, kinks in L-I characteristics are observed.

For simple analysis, it can be assumed that multi-modes within the same LD are not coherent with each other and the overall near- or far-field pattern of the LD is determined by simply adding the intensities of all the modes, which results in symmetric near- and far-field patterns. However, in certain conditions, some of the LD modes can be coherently coupled with each other and result in changes in the carrier concentration (or optical gain) in the cavity and the interference in the output [16]. The exact condition for this is very difficult to determine, but its influence can be observed in L-I kinks as well as in the asymmetric far-field pattern with the resulting beam steering [17]. Although L-I kinks and the corresponding beam steering can significantly affect the applicability of HPLDs, reports on detailed investigations of their relationship are not available. In this paper, we provide the results of such an investigation in which the lateral

*Corresponding author: wchoi@yonsei.ac.kr, ORCID 0000-0003-0067-4657

Color versions of one or more of the figures in this paper are available online.

pISSN: 2508-7266 / eISSN: 2508-7274 https://doi.org/10.3807/COPP.2022.6.2.191

far-field characteristics of 850 nm GaAs/AlGaAs HPLDs with a narrow emitter width are measured at varying output power levels and analyzed. This paper is organized as follows. In Section II, we describe the target 850 nm HPLD used in our investigation. In Section III, we present how the lateral far-field divergence angle changes with the LD output power and provide explanations for their dependence. In section IV, we conclude the paper.

II. DEVICE STRUCTURE AND L-I CHARACTERISTICS

Figures 1(a) and 1(b) respectively show the device structure and a band diagram of the 850 nm LD investigated in this study. It is a ridge waveguide AlGaAs-based LD grown on a GaAs substrate by metalorganic chemical vapor deposition (MOCVD). It contains a 7 nm GaAs single quantum well, AlGaAs barriers, and graded refractive index separate confinement heterostructures. P-type and n-type AlGaAs layers are used as top and bottom cladding layers. The ridge waveguide is formed by wet etching and has a top width of 2.4 μm and bottom width of 4.6 μm, as determined from the SEM image of a fabricated device shown in the inset of Fig. 1(a). Devices with cavity lengths (L) of 1200, 1500 μm, with AR coating for one side (R = 0.03) and HR coating for the other side (R–1), are fabricated, and their characteristics are measured.

Kinks are observed in L-I characteristics, whose relationship with the lateral far-field characteristics is investigated in this paper. Figure 2(a) shows the measured L-I characteristics. Each threshold current is 35 and 40 mA and the output power when kink occurs at 326 and 403 mW and ends at 394 and 497 mW. From the measured L-I characteristics, the internal quantum efficiency η_i and the loss α_i can be estimated as 0.95 for η_i and 3 cm^{-1} for α_i by plotting the inverse of measured slope efficiency against the cavity length as shown in Fig. 2(b).

III. LATERAL FAR-FIELD CHARACTERISTICS

Figures 3(a) and 3(b) show the measured divergence angles of the lateral far-field pattern at various output powers for devices with two different cavity lengths. The

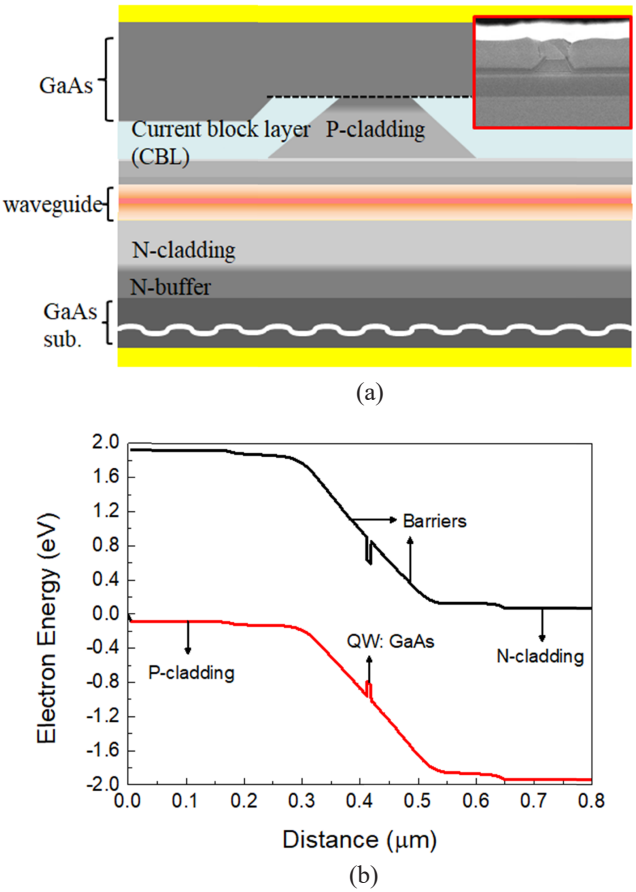

FIG. 1. Laser diodes (LD) structure of the 850 nm LD: (a) cross section, (b) band diagram.

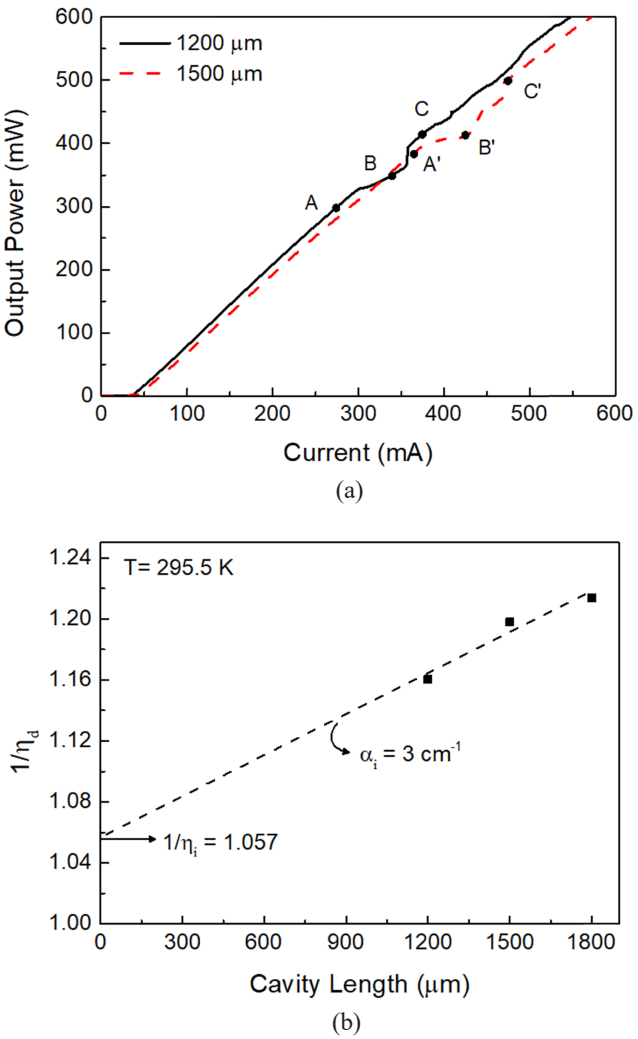

FIG. 2. Measured (a) L-I characteristics, (b) estimation of internal quantum efficiency and loss at T = 295.5 K.

divergence angle is defined as the far-field width when the output power is at $1/e^2$ of the peak. Also shown are the measured far-field patterns at two different output power levels for each device. The output power level points (A, C, A′, and C′) can be identified in the L-I characteristics given in Fig. 2(a).

Figures 3(a) and 3(b) show that the overall divergence angle increases with the HPLD output power because of the occurrence of first-order lateral mode and the enhanced lateral wave confinement due to thermal lensing effect [18–20] by the increased internal device temperature difference between the center and edge of the device. In particular, at power of more than 150 mW, the thermal lensing effect is analyzed as the main cause of the increase in the divergence angle, because it tends to increase quadratically except for the section where the kink occurs in Fig. 3. This trend is similar to the tendency of increasing the internal temperature of the device to be analyzed later. In addition, jumps in the divergence angle are observed when the HPLD output powers are roughly 150 mW for both types of HPLDs. That can be explained by the appearance of the first-order lateral mode at around the output power level. A numerical simulation is conducted for the L-I characteristics to confirm the experiment results as shown in Figs. 4(a) and 4(b). In order to realize accurate simulation results, numerical values for key device parameters are experimentally extracted using the technique described in [21]. As can be seen in Fig. 4, good agreement between measured and simulated L-I characteristics except for kinks is achieved. With simulation, the light output powers due to the fundamental lateral mode and the first-order lateral mode can be separated, and the results are shown in Figs. 4(a) and 4(b). As can be seen for both types of devices, the first-order lateral mode appears when the total output power is roughly 150 mW, corroborating the increase in the measured divergence angle at this output power level in Fig. 3.

In order to make sure that our HPLD simulation is accurate, especially for the internal device temperature that has a strong influence on HPLD far-field pattern character-

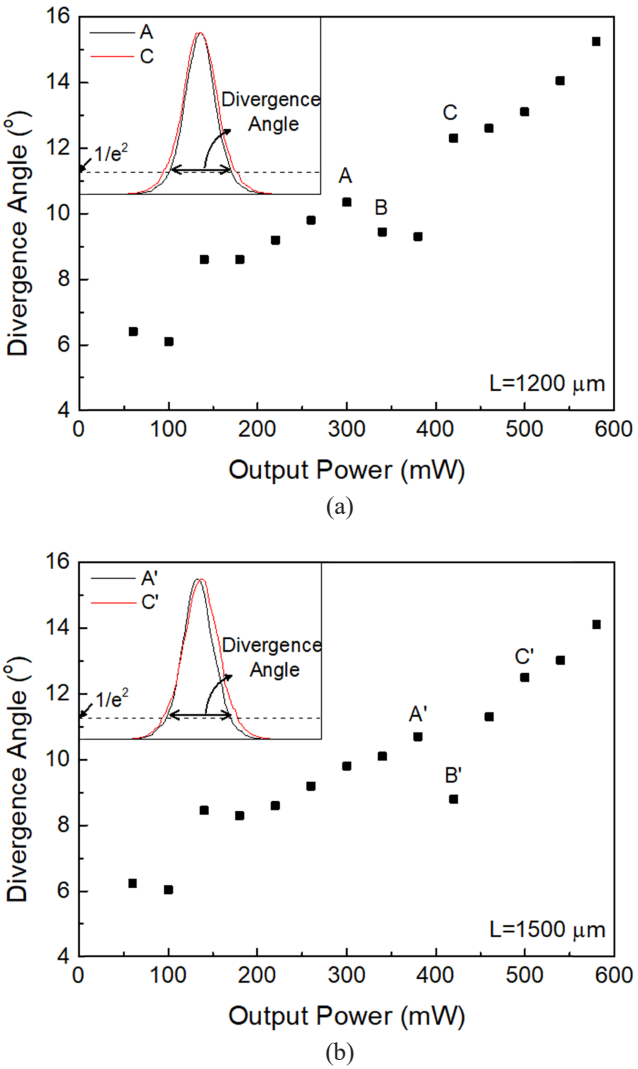

FIG. 3. Measured divergence angle versus output power: (a) L = 1200 and (b) 1500 μm.

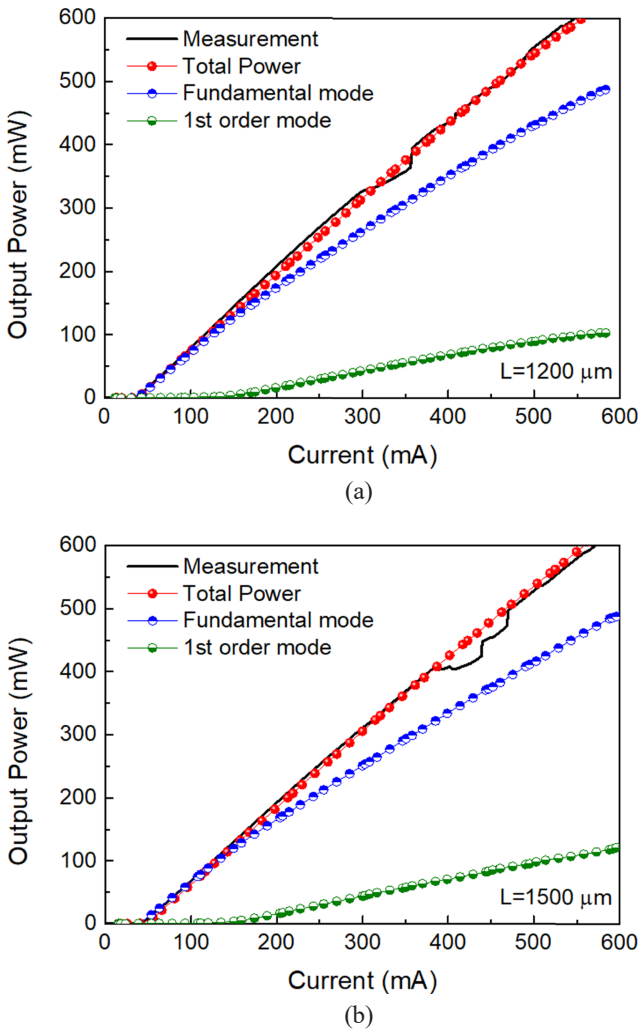

FIG. 4. Measured and simulated L-I curves: (a) L = 1,200 and (b) 1,500 μm.

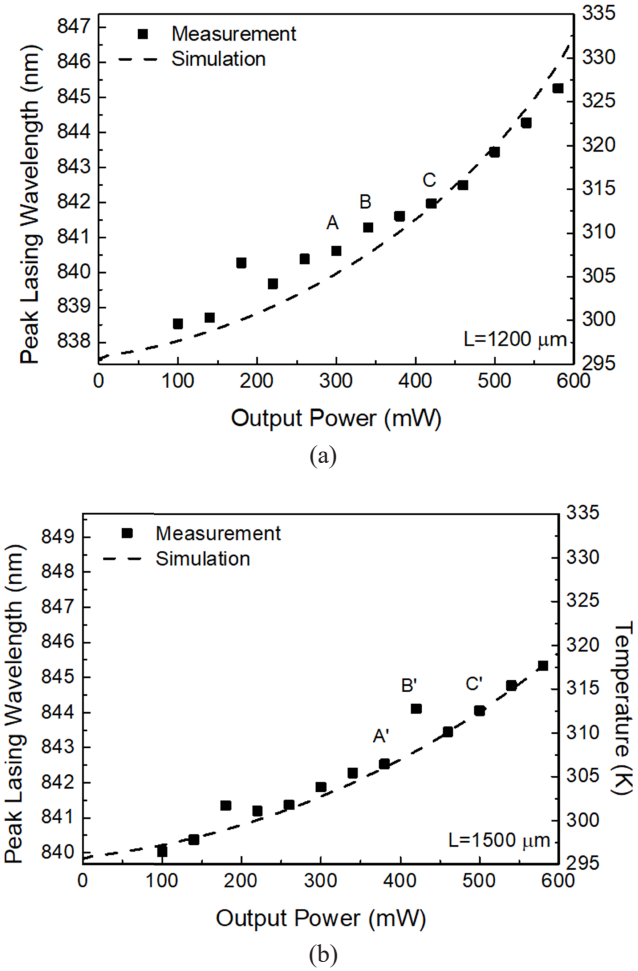

FIG. 5. Measured and simulated peak lasing wavelength and internal temperature versus output power: (a) L = 1200 and (b) 1500 μm.

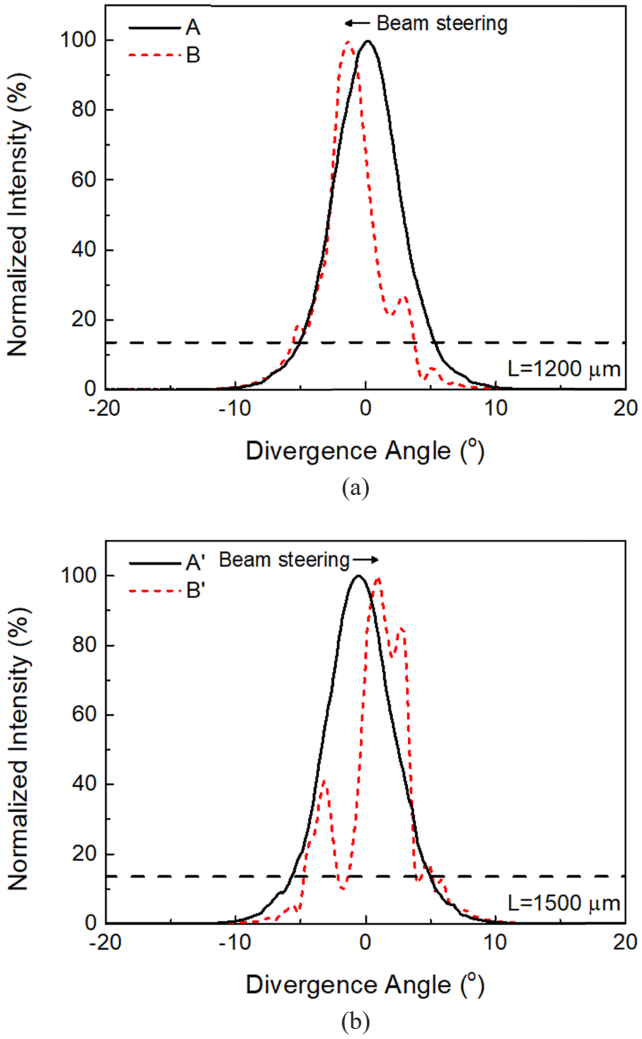

FIG. 6. Measured lateral far-field patterns of kink and pre-kink: (a) L = 1200 and (b) 1500 μm.

istics, we measured the peak lasing wavelengths at different lasing powers [shown with filled squares in Figs. 5(a) and 5(b)]. Then we converted these into the internal device temperature using the measured amount of the peak lasing wavelength shift due to the device temperature change (0.25 nm/K). As shown in Fig. 5, these estimated HPLD internal temperatures agree reasonably well with the simulated results. The injected electrical power is converted into light or heat and each converted optical power and injected electrical power is proportional to the injected current and current square. Therefore, the converted heat is expected to increase quadratically as converted optical power (or output power) increases, and it is shown in Fig. 5.

In Figs. 3(a) and 3(b), a sudden drop in the divergence angle is observed when the output power reaches the kink points (B and B′). Figures 6(a) and 6(b) show that the measured far-field patterns in these conditions have a considerable amount of lateral asymmetry of the beam steering. For comparison, the measured far-field patterns for points A and A′ below the kink condition are also shown.

This observation that kinks in L-I characteristics have corresponding far-field patterns that are steered and narrower can be explained by the coherent superposition from constructive and destructive interferences between the fundamental and the first-order lateral modes. Additionally, it should be noted that in our devices, the kink happens only in a specific range of internal temperature from 307 to 312 K in Fig. 5, the reasons for which require further investigation.

IV. CONCLUSION

We have investigated the lateral far-field characteristics of 850 nm GaAs/AlGaAs HPLD with a narrow emitter width. We experimentally found that the measured far-field patterns change with the output power level, the appearance of the higher-order lateral mode, and the coherent superposition of lateral modes strongly related to the kink in L-I characteristics. These results should be useful information for realizing narrow emitter width HPLDs with good far-field patterns.

FUNDING

Research Fund of High Efficiency Laser Laboratory of the Agency for Defense Development of Korea (NO. UD190015ID).

DISCLOSURES

The authors declare no conflicts of interest.

DATA AVAILABILITY

Data underlying the results presented in this paper are not publicly available at the time of publication, which may be obtained from the authors upon reasonable request.

REFERENCES

1. L. Mei and M. Brydegaard, "Continuous-wave differential absorption lidar," Laser Photonics Rev. **9**, 629–636 (2015).
2. X. Ai, R. Nock, J. G. Rarity, and N. Dahnoun, "High-resolution random-modulation cw lidar," Appl. Opt. **50**, 4478–4488 (2011).
3. J. Yang, G. Zhou, X. Yu, and W. Zhu, "Design and implementation of power supply of high-power diode laser of LIDAR onboard UAV," in *Proc. 2011 International Symposium on Image and Data Fusion* (Tengchong, China, Aug. 9-11, 2011), pp. 1–4.
4. E. Watanabe, N. Arima, and K. Kodate, "Facial recognition system with compact optical parallel correlator using vertical-cavity surface-emitting laser array module," Jpn. J. Appl. Phys. **43**, 5890–5896 (2004).
5. J. Gwak, J. Park, J. Park, K. Baek, A. Choi, and T. Kim, "940-nm 350-mW transverse single-mode laser diode with AlGaAs/InGaAs GRIN-SCH and asymmetric structure," Curr. Opt. Photonics **3**, 583–589 (2019).
6. G. An, Y. Wang, J. Han, H. Cai, Z. Jiang, M. Gao, S. Wang, W. Zhang, H. Wang, L. Xue, and J. Zhou, "Deleterious processes of a diode-pumped cesium vapor hollow-core photonic-crystal fiber laser," High Power Laser Sci. Eng. **4**, e37 (2016).
7. D. A. VinoKurov, V. A. Kapitonov, A. V. Lyutetskiy, D. N. Nikolaev, N. A. Pikhtin, S. O. Slipchenko, A. L. Stankevich, V. V. Shamakhov, L. S. Vavilova, and I. S. Tarasov, "850-nm diode lasers based on AlGaAsP/GaAs heterostructures," Semiconductors **46**, 1321–1325 (2012).
8. S. Banerjee, P. Mason, J. Phillips, J. Smith, T. Butcher, J. Spear, M. D. Vido, G. Quinn, D. Clarke, K. Ertel, C. Hernandez-Gomez, C. Edwards, and J. Collier, "Pushing the boundaries of diode-pumped solid-state lasers for high-energy applications," High Power Laser Sci. Eng. **8**, e20 (2020).
9. Y. Jeong, J. K. Sahu, D. N. Payne, and J. Nilsson, "Ytterbium-doped large-core fiber laser with 1.36 kW continuous-wave output power," Opt. Express **12**, 6088–6092 (2004).
10. L. Zhong and X. Ma, "Recent developments in high power semiconductor diode lasers," in *Optoelectronics: Devices and Applications*, P. Predeep, Ed., (Intechopen, 2011), pp. 325–348.
11. F. Daiminger, F. Dorsch, and D. Lorenzen, "High-power laser diodes, laser diode modules, and their applications," Proc. SPIE **3682**, 13–23 (1998).
12. A. V. Aluev, A. M. Morozyuk, M. S. Kobyakova, and A. A. Chel'nyi, "High-power 2.5-W cw AlGaAs/GaAs laser diodes," Quantum Electron. **31**, 627–628 (2001).
13. B. L. Volodin, S. V. Dolgy, E. D. Melnik, E. Downs, J. Shaw, and V. S. Ban, "Wavelength stabilization and spectrum narrowing of high-power multimode laser diodes and arrays by use of volume Bragg gratings," Opt. Lett. **29**, 1891–1893 (2004).
14. H. Wenzel, F. Bugge, M. Dallmer, F. Dittmar, J. Fricke, K. H. Hasler, and G. Erbert, "Fundamental-lateral mode stabilized high-power ridge-waveguide lasers with a low beam divergence," IEEE Photonics Technol. Lett. **20**, 214–216 (2008).
15. W. D. Herzog, B. B. Goldberg, and M. S. Ünlü, "Beam steering in narrow-stripe high-power 980-nm laser diodes," IEEE Photonics Technol. Lett. **12**, 1604–1606 (2000).
16. L. Brovelli and C. S. Harder, "Laser device," European Patent EP1012933A1 (2000).
17. J. Nappi, A. Ovtchinnikov, H. Asonen, P. Savolainen, and M. Pessa, "Limitations of two-dimensional passive waveguide model for λ=980 nm Al-free ridge waveguide lasers," Appl. Phys. Lett. **64**, 2203–2205 (1994).
18. J. Piprek, "Self-consistent far-field blooming analysis for high-power Fabry-Perot laser diodes," Proc. SPIE **8619**, 861910 (2013).
19. J. Piprek, "Self-consistent analysis of thermal far-field blooming of broad-area laser diodes," Opt. Quantum Electron. **45**, 581–588 (2013).
20. P. Crump, S. Boldicke, C. M. Schultz, H. Ekhteraei, H. Wenzel, and G. Erbert, "Experimental and theoretical analysis of the dominant lateral waveguiding mechanism in 975 nm high power broad area diode lasers," Semicond. Sci. Technol. **27**, 045001 (2012).
21. J. Yang, J. Kwak, A. Choi, T. Kim, and W. Choi, "Analysis of lateral-mode characteristics of 850-nm MQW GaAs/(AL,Ga) as laser diodes," Korean J. Opt. Photon. **30**, 55–61 (2021).